Mechatronics 73 (2021) 102488

Contents lists available at ScienceDirect

Mechatronics

journal homepage: www.elsevier.com/locate/mechatronics

Sensitivity-based data fusion for optical localization of a mobile robot☆

Jason N. Greenberg *, Xiaobo Tan

Smart Microsystems Laboratory, Department of Electrical and Computer Engineering, Michigan State University, East Lansing, MI, 48824, USA

ARTICLE INFO

Keywords:
Robot localization
Triangulation
Optical localization

ABSTRACT

Acoustic-based techniques are the standard for localization and communication in underwater environments, but due to the challenges associated with this medium, it is becoming increasingly popular to find alternatives such as using optics. In our prior work we developed an LED-based Simultaneous Localization and Communication (SLAC) approach that used the bearing angles, needed for establishing optical line-of-sight for LED-based communication between two beacon nodes and a mobile robot, to triangulate and thereby localize the position of the robot. Our focus in this paper is on how to optimally fuse measurement data for optical localization in a network with multiple pairs of beacon nodes to obtain the target location. We propose the use of a sensitivity metric, designed to characterize the level of uncertainty in the position estimate with respect to the bearing angle error, to dynamically select a desired pair of beacon nodes. The proposed solution is evaluated with extensive simulation and experimentation, in a setting of three beacons nodes and one mobile node. Comparison with multiple alternative approaches demonstrates the efficacy of the proposed approach.

1. Introduction

The position of a mobile robot is valuable information needed in a variety of autonomous robot tasks, such as navigation and environmental mapping [1]. Robots working in a group can collaboratively share data amongst themselves in order to localize individual agents of the group. One of these collaborative localization approaches is triangulation, which uses angles relative to several neighbors with known positions, often referred to as beacons (or base nodes), to localize the individual robot [2].

Localization through triangulation is a large field with many implementation techniques in both robotics and surveying engineering, with the latter field referring to triangulation as the three-point resection problem [3]. In their comprehensive review of the subject Pierlot and Van Droogenbroeck grouped these many approaches into four general categories, Geometric Circle Intersection, Iterative methods, Geometric Triangulation, and Multiple Beacons Triangulation, with one of the more commonly used approaches being Geometric Circle Intersection [4]. In this particular type of triangulation, two arcs are derived from the bearing angles that are between three beacons and a target. Each arc spans between one unique pairing of the beacons and passes through all possible coordinates of the target. Thus the intersection point of two of these arcs leads to the position of the target [3–5].

A form of Geometric Triangulation is implemented by Sergiyenko and coworkers in [6–8] by finding the bearing angles of a laser transmitter and a receiver necessary for the receiver to detect the light from the transmitter that is deflected off the object of interest. The transmitter and receiver units are mounted on a beam at a fixed distance apart; this combined with measured angles allows for the Laws of Sines to be used to triangulate the coordinates of the point of deflection on the object.

Sensitivity or error analysis of triangulation methods to improve certain aspects of the system has been done previously [3,9,10]. Tekdas and Isler [9] used a common uncertainty function to implement a beacon placement algorithm and Font-Llagunes and Batlle [3] presented an error analysis of their triangulation method to also generalize a preferred configuration of beacons. However, in both works the analysis is used to only create a static solution and is not used to dynamically improvise the measurement process to adapt to changes in robot location. A dynamic approach was developed by Madsen et al. [10] for their robot self-positioning triangulation technique, in which the position of the robot was computed from the angles of separation between the landmarks, i.e., points of interest, detected by a camera. Their method employed a specially designed metric that characterized the relationship between the error in locating the positions of landmarks in the captured image and the error in the computed robot position. This metric would then be used to find the best landmark triplet, within

☆ This paper was recommended for publication by Associate Editor Alexander Leonessa.

* Corresponding author.
E-mail addresses: green108@egr.msu.edu (J.N. Greenberg), xbtan@msu.edu (X. Tan).

https://doi.org/10.1016/j.mechatronics.2021.102488
Received 11 November 2019; Received in revised form 7 December 2020; Accepted 30 December 2020
Available online 9 January 2021

an environment that had many landmarks, to best localize the robot at each point in its trajectory.

A noticeable advantage of group-based localization methods is an ability to be functional in environments where GPS signals are inaccessible such as indoors and underwater. Underwater implementations are often challenged by the poor signal quality of acoustic-based methods, which are the current standard solutions for localization and communication in the underwater environment. In particular, the long propagation delays, limited bandwidth, and the multipath effect of acoustic signals, which often result in low signal reception reliability and low data rates, make working with them very difficult [11–14]. Alternatives to acoustic approaches have been explored, including optical-based approaches such as those using Light-Emitting Diodes (LEDs). However, a near line-of-sight (LOS) between transmitter and receiver is needed for LED-based approaches to operate; several methods, such as the use of redundant transmitters/receivers [15–18] and active alignment [19–21] have been proposed to address this challenge.

In our earlier work, [22–24], a solution to Simultaneous Localization and Communication (SLAC) using an LED-based optical system was proposed. Localization was accomplished using the bearing angles needed to establish optical LOS between two base nodes (or beacons) with known positions and a mobile robot. In particular, these bearing angles were captured by the base nodes and then used to compute the robot's position via triangulation. Critical to the success of the localization, the maintenance of the LOS between the base nodes and mobile robot, is made difficult due to the robot's mobile nature. To address this challenge, the robot's next set of coordinates were predicted with a Kalman filter, which helped to minimize the effort needed to measure the bearing angles and allowed for a dynamic localization approach. One glaring drawback to this approach of using two base nodes, is that, when the mobile robot is close to forming a collinear configuration with the base nodes, a singularity issue arises with the position measurement.

This work explores the optical localization of a mobile robot using a group of (more than two) base nodes, with the main focus set on finding the best way to fuse the data from the multiple sources so to enhance the positioning accuracy. One of the goals of the proposed work is to address the singularity limitation of the two-base-node method. The redundancy from extra nodes could present alternative base-node pairings when one or more pairings are in a collinear configuration with the robot. An important design consideration is how to fuse the additional bearing angle information effectively. This work proposes the use of a sensitivity metric, which represents how sensitive a triangulated position is with respect to the bearing measurement error, to choose a pair of base nodes for triangulation that are the most robust at that time instance. In particular, the base node pairing with the lowest sensitivity metric is chosen to compute the target's position using the corresponding measured bearings. The resulting position is then fed into the Kalman filter to predict the target's next position, which is critical for facilitating the LOS establishment for the next round of communication and localization.

Preliminary results for the proposed method were presented at the 2019 IEEE/ASME International Conference on Advanced Intelligent Mechatronics (AIM) [25]. The work presented here is a significant extension to [25] with new simulation analysis and extensive experimental results, including comparison with additional alternative approaches.

Both the simulation and experimentation compare the performance of our proposed sensitivity metric-based approach against three alternatives methods. These three approaches include a different means of data fusion in the form of averaging the triangulated target positions computed from the bearing angles of each base node pairing, a variation to the filtering scheme by incorporating the current angle measurements in the measurement noise covariance matrix, and a combination of the averaging fusion technique with this filtering scheme variation. A fourth alternative approach is also examined in simulation, in which the captured bearing angles are used directly as the system output and are nonlinear functions of the states, thereby entailing the use of an extended Kalman filtering (EKF) scheme [26].

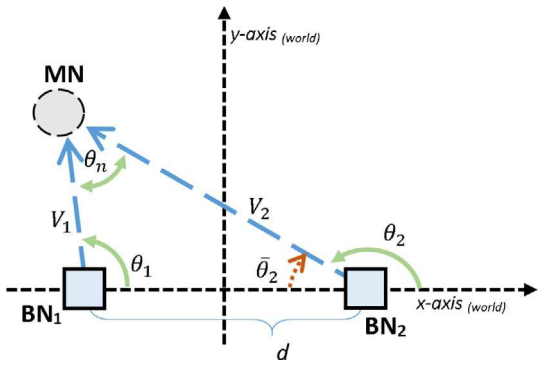

Fig. 1. Illustration of the geometric triangulation used in the two-base-node approach.

Results show that the proposed sensitivity metric-based approach outperforms the alternative variations and achieves an average estimated position error of roughly 0.18 grid units in experiments, whereas the alternative averaging and filtering scheme approaches achieve average estimated position errors of approximately 0.19, 0.28, and 0.25 grid units in experiments, respectively. The alternative EKF-based approach yielded relatively poor results with the estimated velocity diverging away from the ground truth fairly quickly, thereby causing the system to consequently fail at maintaining the LOS.

The remainder of this paper is organized as follows. Section 2 reviews the position triangulation technique and Kalman filtering for the setting of two base nodes and one mobile node (target). Section 3 details the sensitivity metric and the proposed fusion approach. Simulation results are provided in Section 4, followed by experimental evaluation in Section 5. Finally, conclusion and future work are discussed in Section 6.

2. The two-base-node localization approach

2.1. Measurement process

The approach discussed in this work has been designed in the two-dimensional (2D) setting. The two-base-node approach involves a three-node network, consisting of a mobile node (MN) to be localized and a single pair of base nodes (with known locations, BN_1 and BN_2) as shown in Fig. 1.

Each node has a photodiode receiver and an LED transmitter as components of its optical transceiver, which is able to rotate 360° and keep track of the changes in its orientation. As the MN shines its light at each base node, the base nodes rotate their transceivers to determine the LOS measurement with respect to the MN based on the received light intensity, thus extracting their respective bearing angles θ_1 and θ_2. Further details on the scanning process are described in Section 2.2.

Through the use of these angles and the locations of the base nodes, the mobile node's x and y coordinates are computed as:

$$\begin{bmatrix} n_x \\ n_y \end{bmatrix} = \begin{bmatrix} B_{1x} + |V_1| \cos\theta_1 \\ B_{1y} + |V_1| \sin\theta_1 \end{bmatrix} \tag{1}$$

where $\left[B_{1x},\ B_{1y}\right]^T$ and $\left[n_x,\ n_y\right]^T$ are the position vectors of BN_1 and the mobile node MN, respectively, and $|V_1|$ is the magnitude of vector V_1 shown in Fig. 1 and is obtained using the Laws of Sines. In particular,

$$|V_1| = \frac{d\ \sin(\bar{\theta}_2)}{\sin(\theta_n)} \tag{2}$$

where the value of $\bar{\theta}_2$ is the complement of θ_2, $\bar{\theta}_2 = 180° - \theta_2$, θ_n is an angle, within the MN-BN_1-BN_2 triangle, that corresponds to the side BN_1-BN_2, $\theta_n = \theta_2 - \theta_1$, and d is the length of the side BN_1-BN_2.

Despite the seemingly straightforward static measurement process shown in Fig. 1, using it to localize a mobile target can be especially challenging, since this can easily lead to an inadequate LOS for measurements caused by insufficient synchronization and coordination among all of the nodes. There is also the complication of relying on pure algebraic calculations for the position (1), since the inherent noise in the measurement angles will lead to highly variable (instead of smooth) estimated trajectories for the mobile node MN.

Kalman filtering addresses this issue by exploiting the predicted positions of the MN it generates from the robot's dynamics and the measurements computed by (1), to significantly reduce the effort of searching for the LOS and thus enabling efficient, accurate, and dynamic localization. In particular, the predicted position is used to generate anticipated angular locations of the mobile node, $\hat{\theta}_{i,k}$ (recall Fig. 1), relative to each ith base node, which are then used to center the scanning process of that base node. These angles are computed as follows:

$$\hat{\theta}_{i,k} = \cos^{-1}\left(\frac{V_b \cdot V_{m_i}}{|V_b|\,|V_{m_i}|}\right)$$

where, $V_b = \begin{bmatrix}1\\0\end{bmatrix}$, $\quad V_{m_i} = \begin{bmatrix}\hat{n}_x^-\\ \hat{n}_y^-\end{bmatrix} - \begin{bmatrix}B_{ix}\\ B_{iy}\end{bmatrix}$

Here $\left[B_{ix},\ B_{iy}\right]^T$ are the position coordinates of the ith base node $\mathrm{BN_i}$, $V_b \cdot V_{m_i}$ is the dot product between vectors V_b and V_{m_i}, and $\left[\hat{n}_x^-,\ \hat{n}_y^-\right]^T$ is the predicted position vector of the MN.

The designs of the proposed position measurement-based Kalman filtering algorithm as well as an alternative angle measurement-based extended Kalman filtering algorithm are presented next.

2.2. The Kalman filtering algorithms

The main purpose for using Kalman filtering in this work is to facilitate the maintenance of the line of sight between the base nodes and the mobile node, by predicting the future positions of the robot so to produce anticipated angles for the transceiver orientation. It is assumed that the dynamics of the mobile node are captured with a constant velocity model corrupted with Gaussian noise, since precise prior knowledge of the mobile node's movement would in general not be available to the base nodes. Potentially, alternative filtering and predictive schemes, such neural networks [27], could have been used. However, the assumption on the dynamics enables the use of computationally efficient Kalman filtering for predicting the mobile node's coordinates. Moreover, other approaches tend to require additional overhead; for example, in the case of neural networks one needs to train the system in advance.

The dynamics for the mobile node can be represented as:

$$\boldsymbol{n}_{k+1} = \boldsymbol{n}_k + \boldsymbol{v}_k \Delta_k + w_{1,k} \tag{3}$$

$$\boldsymbol{v}_{k+1} = \boldsymbol{v}_k + w_{2,k} \tag{4}$$

where $\boldsymbol{v}_k = \left[v_{x,k},\ v_{y,k}\right]^T$ and $\boldsymbol{n}_k = \left[n_{x,k},\ n_{y,k}\right]^T$ are the velocity and position vectors of the mobile node at the kth time instance, $w_{1,k}$ and $w_{2,k}$ are independent, zero-mean, white Gaussian noises, and Δ_k is the kth sampling interval.

A state vector $\mathbf{x}_k$ is used in the Kalman filter and is comprised of $\boldsymbol{n}_k$ and $\boldsymbol{v}_k$ stacked together, in particular:

$$\mathbf{x}_k = \left[n_x,\ n_y,\ v_x,\ v_y\right]^T \tag{5}$$

With this state vector, (3) and (4) can be rewritten as:

$$\mathbf{x}_{k+1} = A_k \mathbf{x}_k + \left[w_{1,k}, w_{2,k}\right]^T \tag{6}$$

where A_k is the matrix derived from the mobile node's motion model (3) and (4):

$$A_k = \begin{bmatrix}1 & 0 & \Delta_k & 0\\ 0 & 1 & 0 & \Delta_k\\ 0 & 0 & 1 & 0\\ 0 & 0 & 0 & 1\end{bmatrix}$$

The next predicted state and error covariance are generated with:

$$\hat{\mathbf{x}}_k^- = A_{k-1}\hat{\mathbf{x}}_{k-1} \tag{7}$$

$$\hat{\mathbf{P}}_k^- = A_{k-1}\hat{\mathbf{P}}_{k-1}A_{k-1}^T + Q_{k-1} \tag{8}$$

where $\hat{\mathbf{x}}_{k-1}$ is the previous state estimate, $\hat{\mathbf{x}}_k^-$ is the *a priori* state estimate, $\hat{\mathbf{P}}_k^-$ is the predicted state covariance matrix, and Q_k is the process noise covariance matrix.

This work will consider two Kalman filtering schemes. In the scheme that is proposed, the observation, $\mathbf{z}_k$, is considered to be a noise-corrupted position measurement (derived from the raw bearing angle measurements). In the alternative scheme, the observation, $\boldsymbol{\zeta}_k$, is a pair of noise-corrupted angles captured directly from the measurement process.

2.2.1. Position-based Kalman filtering

The noise-corrupted position observation, $\mathbf{z}_k$, is computed based on (1):

$$\mathbf{z}_k = \boldsymbol{n}_k + w_{3,k}, \tag{9}$$

where $w_{3,k}$ is assumed to be a white, zero-mean Gaussian noise, and independent of the process noises $w_{1,k}$ and $w_{2,k}$. The physical implementation of the position measurement (9) is through the triangulation of the measured bearing angles. In [24] we showed through simulation that the noise in the position measurement exhibits a Gaussian form when the noise applied to the bearing angles is uniform or Gaussian, thus justifying our use of Gaussian noise in this position measurement model.

This position measurement (9) can also be rewritten in terms of the state vector as:

$$\mathbf{z}_{k+1} = H_k \mathbf{x}_k + w_{3,k} \tag{10}$$

where $\mathbf{H}_k$ is the observation matrix:

$$\mathbf{H}_k = \begin{bmatrix}1 & 0 & 0 & 0\\ 0 & 1 & 0 & 0\end{bmatrix}$$

The observation $\mathbf{z}_k$ is used in the state estimate:

$$\hat{\mathbf{x}}_k = \hat{\mathbf{x}}_k^- + \mathbf{K}_k\left(\mathbf{z}_k - \mathbf{H}_k\,\hat{\mathbf{x}}_k^-\right) \tag{11}$$

where

$$\mathbf{K}_k = \hat{\mathbf{P}}_k^-\mathbf{H}_k^T\left(\mathbf{H}_k\,\hat{\mathbf{P}}_k^-\,\mathbf{H}_k^T + R_k\right)^{-1} \tag{12}$$

$$\hat{\mathbf{P}}_k = \left(\mathbf{I} - \mathbf{K}_k\,\mathbf{H}_k\right)\hat{\mathbf{P}}_k^- \tag{13}$$

$\mathbf{K}_k$ is the Kalman gain, R_k is the covariance matrix of measurement noise, and $\hat{\mathbf{P}}_k$ is the posterior error covariance matrix.

2.2.2. Angle-based extended Kalman filtering

For the alternative scheme, the observation, $\boldsymbol{\zeta}_k$, is expressed as:

$$\boldsymbol{\zeta}_k = \boldsymbol{\Theta}_k + \omega_{4,k}$$

where $w_{4,k}$ is assumed to be a white, zero-mean Gaussian noise, and independent of noises $w_{1,k}$ and $w_{2,k}$ and $\boldsymbol{\Theta}_k = \left[\theta_{a,k},\ \theta_{b,k}\right]^T$ consists of the two bearing angles, $\theta_{a,k}$ and $\theta_{b,k}$, associated with the pair of base nodes, $\mathrm{BN_a}$ and $\mathrm{BN_b}$, used for the measurement at the kth time instance. The physical implementation of this measurement is directly the result of extracting the bearing angles from the scanned light intensities. These angles can be expressed as nonlinear functions of the states:

$$g(n_{x,k},\ n_{y,k}) = \begin{bmatrix}\theta_{a,k}\\ \theta_{b,k}\end{bmatrix} = \begin{bmatrix}g_1(n_{x,k},\ n_{y,k})\\ g_2(n_{x,k},\ n_{y,k})\end{bmatrix}$$

$$= \begin{bmatrix}\cos^{-1}\left(\dfrac{(n_{x,k}-B_{ax})}{\sqrt{(n_{x,k}-B_{ax})^2+(n_{y,k}-B_{ay})^2}}\right)\\ \cos^{-1}\left(\dfrac{(n_{x,k}-B_{bx})}{\sqrt{(n_{x,k}-B_{bx})^2+(n_{y,k}-B_{by})^2}}\right)\end{bmatrix} \tag{14}$$

where $[B_{ax},\ B_{ay}]^T$ and $[B_{ax},\ B_{by}]^T$ are the position vectors of BN_a and BN_b, respectively. This nonlinear relationship between the states and the measurement requires the use of the extended Kalman filtering (EKF) scheme. Consequently, the observation matrix G_k is computed as the Jacobian of function g evaluated at the current predicted position $[\hat{n}^-_{x,k}, \hat{n}^-_{y,k}]$:

$$G_k = \begin{bmatrix}\dfrac{\partial g_1}{\partial n_{x,k}}(\hat{\boldsymbol{n}}^-_k) & \dfrac{\partial g_1}{\partial n_{y,k}}(\hat{\boldsymbol{n}}^-_k) & 0 & 0\\ \dfrac{\partial g_2}{\partial n_{x,k}}(\hat{\boldsymbol{n}}^-_k) & \dfrac{\partial g_2}{\partial n_{y,k}}(\hat{\boldsymbol{n}}^-_k) & 0 & 0\end{bmatrix} \tag{15}$$

where

$$\hat{\boldsymbol{n}}^-_k = \begin{bmatrix}\hat{n}^-_{x,k}\\ \hat{n}^-_{y,k}\end{bmatrix} \tag{16}$$

The state estimate is then computed as:

$$\hat{\mathbf{x}}_k = \hat{\mathbf{x}}^-_k + \mathbf{K}_k\left(\zeta_k - g(\hat{n}_k)\right) \tag{17}$$

where

$$\mathbf{K}_k = \hat{\mathbf{P}}^-_k \mathbf{G}^T_k \left(\mathbf{G}_k\,\hat{\mathbf{P}}^-_k\,\mathbf{G}^T_k + R_a\right)^{-1} \tag{18}$$

$$\hat{\mathbf{P}}_k = \left(\mathbf{I} - \mathbf{K}_k\,\mathbf{G}_k\right)\hat{\mathbf{P}}^-_k \tag{19}$$

$\mathbf{K}_k$ is the Kalman gain, R_a is the covariance matrix of angle measurement noise, and $\hat{\mathbf{P}}_k$ is the posterior error covariance matrix.

3. Sensitivity metric

Increasing the number of base nodes allows the system to capture multiple perspectives of the mobile node's location; however, the challenge then becomes how to best incorporate all of the available information. In this paper, the proposed approach is to use a sensitivity metric to evaluate the level of uncertainty in a computed position based on the level of uncertainty in the pair of measured bearing angles. In particular, this sensitivity metric can be applied to the captured angles of each base node pair in order to characterize the level of uncertainty in the resulting position for that pair. This allows for the position from the base node pair with the lowest level of uncertainty to be used as the location observation, $\mathbf{z}_k$, for that cycle.

In this work the sensitivity metric is defined in terms of the infinity norms of the Jacobians in the x and y directions, $\|J_x\|_\infty$ and $\|J_y\|_\infty$, respectively, of the measurement equation (1) with respect to angles θ_1 and θ_2. Rewritten to be expressed in terms of the angles, (1) becomes $f_x(\theta_1,\theta_2)$ and $f_y(\theta_1,\theta_2)$ where

$$f_x = B_{1x} + \frac{d\ \sin\theta_2}{\sin(\theta_2-\theta_1)}\cos\theta_1 \tag{20}$$

$$f_y = B_{1y} + \frac{d\ \sin\theta_2}{\sin(\theta_2-\theta_1)}\sin\theta_1 \tag{21}$$

Then $\|J_x\|_\infty$ and $\|J_y\|_\infty$ can be defined as:

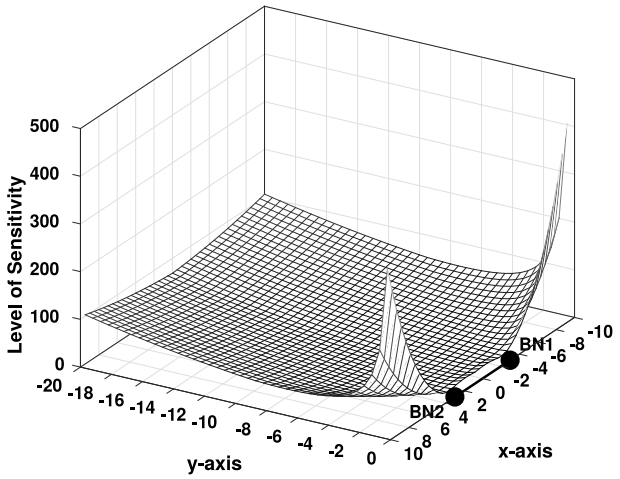

Fig. 2. Illustration of the spatial sensitivity of the two base node measurement function, half symmetry.

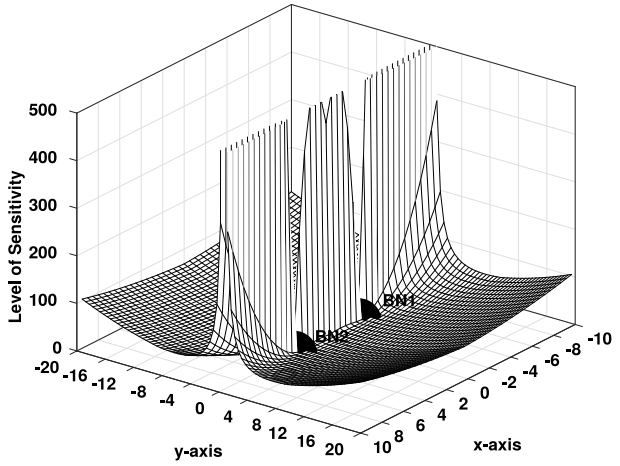

Fig. 3. Illustration of the spatial sensitivity of the two base node measurement function, full symmetry.

$$\|J_x\|_\infty = \left\|\frac{\partial f_x}{\partial\theta_1}\quad\frac{\partial f_x}{\partial\theta_2}\right\|_\infty = \frac{d}{2}\left|\frac{1}{\sin^2(\theta_2-\theta_1)}\right|\max(\left|\sin 2\theta_2\right|,\left|\sin 2\theta_1\right|) \tag{22}$$

$$\|J_y\|_\infty = \left\|\frac{\partial f_y}{\partial\theta_1}\quad\frac{\partial f_y}{\partial\theta_2}\right\|_\infty = d\left|\frac{1}{\sin^2(\theta_2-\theta_1)}\right|\max(\left|\sin^2\theta_2\right|,\left|\sin^2\theta_1\right|) \tag{23}$$

These functions characterize how small changes in the measurement angles for a given pair of base nodes result in changes to the computed position. Visual representations of this uncertainty characterization is shown in Figs. 2, 3, and 4. In Fig. 2 the plot shows the relationship for a range of positions within $x \in [-10, 10]$ and $y \in [0, -20]$ for a pair of base nodes (BN_1, BN_2) located at $[-3, 0]^T$, and $[3, 0]^T$ for BN_1 and BN_2, respectively. In this plot the z-axis indicates the level of sensitivity, calculated as the Euclidean norm of $\|J_x\|_\infty, \|J_y\|_\infty$. A notable observation from this illustration is that the level of sensitivity, and correspondingly the localization uncertainty, is best along the perpendicular bisector of the base nodes with the sensitivity getting worse as the mobile node gets further away from the base nodes and/or deviates away from the bisector. Fig. 2 also shows that the sensitivity is the highest as the mobile node gets closer to being collinear with

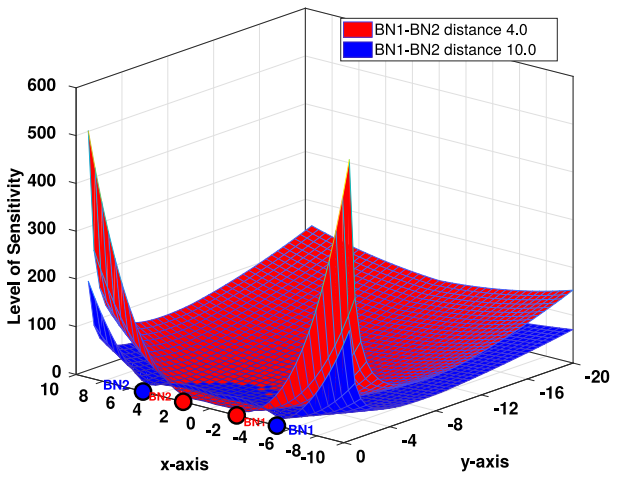

Fig. 4. Illustration comparing the spatial sensitivity of the two base node measurement function when the base nodes are separated by a distance of 4 and 10 grid units.

the base nodes. In Fig. 3 this uncertainty relationship is shown to be symmetric about the collinear axis of the base nodes. Fig. 4 shows how the spatial sensitivity changes with different distances between the two base nodes BN_1 and BN_2. In particular, it shows how the spatial sensitivity maps when the base nodes are separated by a distance of 4 and 10 grid units, respectively. A notable obersvation is that the level of sensitivity generally decreases as the distance between the base nodes increases, with the exception of a small area immediately in front of the base nodes, where the sensitivity is slightly lower when the base nodes are closer together.

In implementation the captured angles from each pair combination of base nodes will be used to evaluate the magnitude of $J = (\|J_x\|_\infty, \|J_y\|_\infty)$, which is the sensitivity metric. The angles from the base node pairing that generates the lowest sensitivity value are used to calculate the observed position $\mathbf{z}_k$, to be used in the Kalman filtering to estimate the mobile node's position.

4. Simulation results

The proposed minimum sensitivity-based data fusion approach uses a constant value, R_c, for its measurement noise covariance matrix, R_k, which was computed in advance using data collected from hardware. It is discussed in detail in Section 5.1.

In simulation this proposed approach is evaluated by comparing it to four alternatives methods, when each method is exposed to a range of angle measurement noises.

4.1. Alternative approaches

Variable-R with minimal sensitivity

In this approach the measurement noise covariance matrix, R_k, is redefined in terms of the variance of the angle measurement and thus varies depending on the mobile robot's current location. In particular, R_k is computed via:

$$R_k = M_k R_a M_k^T \tag{24}$$

where

$$M_k = \begin{bmatrix} \frac{\partial f_x}{\partial \theta_1} & \frac{\partial f_x}{\partial \theta_2} \\ \frac{\partial f_y}{\partial \theta_1} & \frac{\partial f_y}{\partial \theta_2} \end{bmatrix} \tag{25}$$

R_a is the (constant) error covariance matrix of the angle measurement, and f_x and f_y are as defined in (20) and (21), respectively.

The value of M_k is re-computed for each step in the trajectory since it is dependent on the latest angles measured at that step. Just like in the proposed approach, the observed position $\mathbf{z}_k$ is computed from the base node pair with the minimal sensitivity metric. For consistency purposes these same angles are also used to evaluate M_k.

Fixed-R with averaging

For this approach data fusion is achieved by averaging the triangulated positions from each base node pair. As with the proposed approach, the measurement noise covariance matrix, R_k, is set to the constant value, R_c.

Variable-R with averaging

This alternative approach uses both the averaging technique for data fusion and the variable measurement noise covariance matrix that depends on the angles measured from the current trajectory step. To mirror the fact that the observed position $\mathbf{z}_k$ is a blend of all 3 base node pairs, the value of M_k is computed as the average of each instance of (25) that is generated from each pair of base node angles.

Extended Kalman filtering scheme

In this alternative approach, the captured bearing angles are directly used as the system output and are related to the states through nonlinear functions, thereby requiring the use of the extended Kalman Filter (EKF). Similar to the proposed approach, the measurement noise covariance matrix, R_k, is set to a constant value, R_c. However, in this case the value of R_c is built from the variances of the measurement angles' noise.

4.2. Simulation setup

The simulation involves a network that includes 3 base nodes, even though the proposed approach applies to a network with an arbitrary larger number of base nodes. The base nodes are positioned into a configuration where the perpendicular bisector of each base node pair allows near overlapping coverage at any angle relative to the center of the configuration. In particular, the three base nodes, BN_1, BN_2, and BN_3, are stationed at the coordinates $[-3,-3]^T$, $[0,0]^T$, and $[3,-3]^T$, respectively. While other configurations, in particular an equilateral triangle, of the base nodes may potentially have greater coverage capabilities, limited space in the experiment environment makes this difficult to implement while still maintaining sufficient distance between the base nodes.

The trajectory used to evaluate the system is a single loop around all of the base nodes where the direction of the mobile node does not reverse, as shown in Fig. 5.

Simulation of angle measurement errors are achieved with additive independent, zero-mean, white Gaussian noises to each of the ground truth angles, corresponding to the base nodes which are able to establish LOS with the MN during the measurement sequence. By adjusting the standard deviation of the Gaussian noise the level of angle error can be controlled.

4.3. Simulation results

Each of the approaches are evaluated in simulation under different levels of angular measurement error. The standard deviation of the Gaussian noise is ranged from 0.5° to 3.0° in increments of 0.5°, with 200 trials conducted for each level of error. A set of 200 random seeds is used, one seed for each trial, to control the randomness of the simulation so it would be repeatable and consistent across the different levels of angular measurement error.

Fig. 6 compares the average estimated position error for four of the algorithm variations under each level of standard deviation for the angular measurements; the extended Kalman filtering scheme is not included in this plot. The results in the figure show that in general the

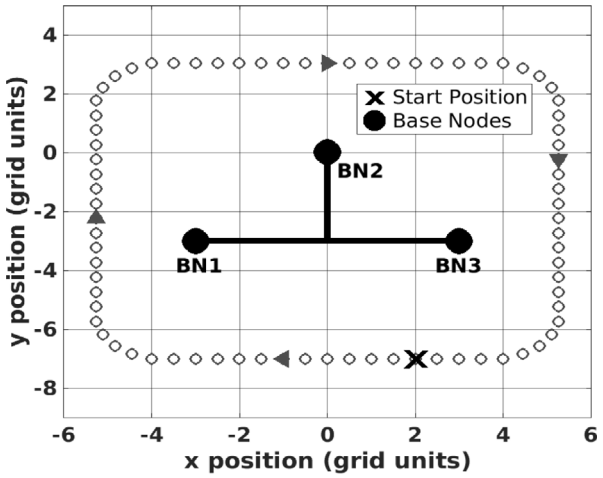

Fig. 5. Illustration of the single loop trajectory with the base nodes, BN_1, BN_2, and BN_3, located at the coordinates $[-3,-3]^T$, $[0,0]^T$, and $[3,-3]^T$, respectively.

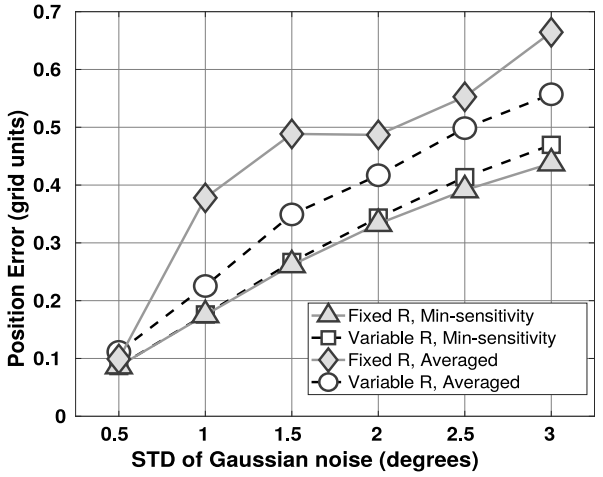

Fig. 6. Line graph showing the average estimated position error for four of the algorithm variations under each level of standard deviation for the angular measurements.

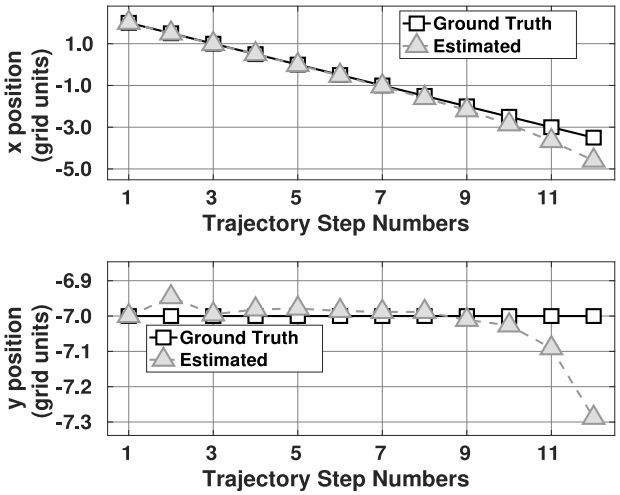

Fig. 7. Simulation results from one of the trials of the angle-based extended Kalman filtering approach in which the angular measurements experienced noise with a standard deviation of 0.5°. The graphs compares the x and y coordinates of the estimated and ground truth positions for each the trajectory steps reached by the system during the trail.

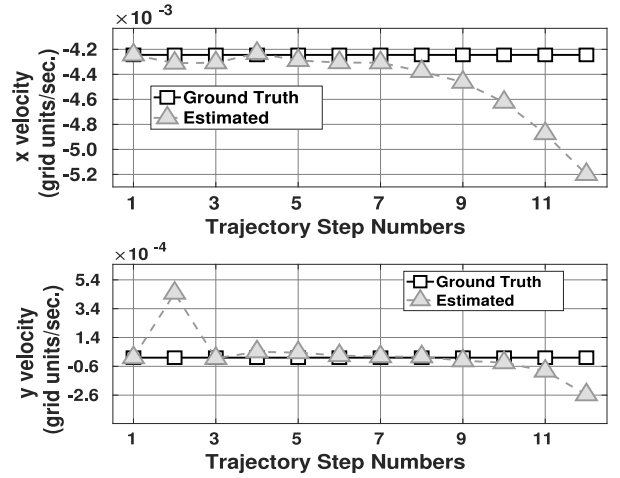

Fig. 8. Simulation results from one of the trials of the angle-based extended Kalman filtering approach in which the angular measurements experienced noise with a standard deviation of 0.5°. The graphs compares the x and y coordinates of the estimated and ground truth velocities for each the trajectory steps reached by the system during the trail.

proposed minimal sensitivity algorithm out performs both cases of the averaged-based fusion technique. Both cases of the minimal sensitivity algorithm show very similar performance output, with the proposed fixed-R approach showing a slight advantage over the variable-R approach as the level of standard deviation for the angle measurement error gets larger.

Results from the angle-based extended Kalman filtering approach are shown in Figs. 7 and 8, which compare the estimated position and estimated velocity against their ground truth counterparts, respectively. The results shown are from a single simulated trial in which the angular measurement noise had a standard deviation of 0.5°. The figures show that the velocity estimates diverge from the ground truth fairly early-on in the trajectory, which causes the position estimates to suffer, resulting in the system failing to maintain the LOS between the mobile and base nodes any further. The latter observation indicates that this EKF approach was only able to localize until trajectory step 12 of 78, roughly 15% of the entire trajectory, which is not surprising since the stability of an EKF is not guaranteed in general. Based on this, this approach is not further tested in experiments.

5. Experimental results

5.1. Setup

The nodes used in the experiments were each equipped with an LED (CREE XRE 1 Watt Blue LED, transmitter) and photodiode (Blue Enhanced photodiode, receiver) which were connected to a circular PCB board with the transceiver circuitry developed by Al-rubaiai in [20]. The circuit processed the light intensity received by the photodiode into a readable analog voltage and enabled quick switching of the LED so to modulate the transmitted baud rate of serial communication. A through hole slip ring was used to allow the shaft of a stepper motor to connect to the transceiver PCB board so that the wires that connected this circuit to the embedded controller could move freely while the stepper motor rotated the PCB board. The motor and slip ring were mounted together via a 3D-printed base structure [25]. Fig. 9 illustrates the locations of these components on a generic node.

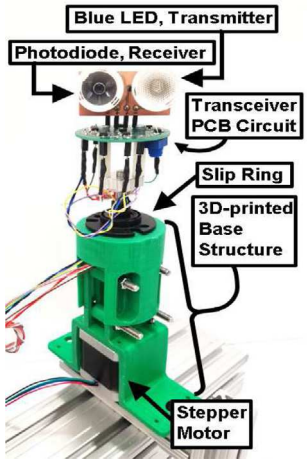

Fig. 9. LED transceiver mounted on each node.

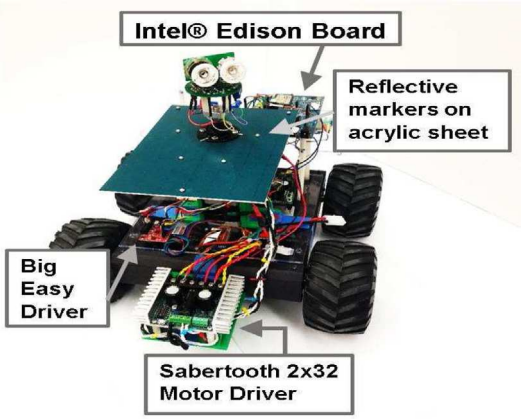

Fig. 10. The mobile node had an acrylic sheet with reflective markers for capturing the position and orientation of the rover.

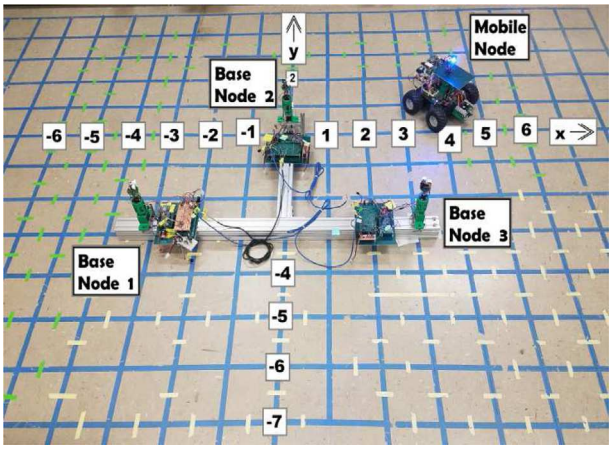

Fig. 11. Overhead view of the grid floor used in experiments. (For interpretation of the references to colour in this figure legend, the reader is referred to the web version of this article.)

Each node used an Intel® Edison Board with an Arduino® Expansion Board for the embedded controller. Equipped with a 500 MHz Intel® Atom dual-core processor with 1 GB of DDR3 RAM, and a built-in dual-band 2.4 GHz and 5 GHz Broadcom® 43340 802.11 a/b/g/n Wi-Fi adapter, the Intel® Edison Board managed stepper motor rotation, LED signal transmission and reception, and Kalman filter processing.

Rotation of the transceiver was achieved with the Intel® Edison Board sending step pulses to the stepper motor driver which translated the pulses and rotated the stepper motor. The particular driver used was a Sparkfun® Big Easy Driver and was set to the quarter step mode (i.e. each step rotated the shaft 0.225°). Awareness of the orientation of the node's transceiver was maintained by the Intel® Edison Board which kept count of the number of clockwise and counter-clockwise steps sent to the driver.

To maintain the fixed positions of the base nodes, the 3D-printed base of each node was mounted on the top of a 80/20® metal beam. Similarly for the mobile robot its 3D-printed base was mounted on the top of a Lynxmotion® Aluminum 4WD1 Rover Kit as shown in Fig. 10. The mobile node and base nodes are shown together in Fig. 11 on the grid used for conducting the experiments. The grid pattern shown was laid out with blue painters tape which followed the grout in the tiles on the floor. Each square in the grid had a side length of approximately 23 cm and was used to represent 1 grid unit, which was used as a generic unit of length to measure motion and position.

Each base node captured their own angles independently, and since the computations of the Kalman filter were done entirely on BN_3, the data collected by BN_1 and BN_2 were transmitted back to BN_3 via a physical three-wire Universal Asynchronous Receiver/Transmitter (UART) network. In addition to exchanging angle data, the UART network enabled BN_3 to orchestrate the actions of the other base nodes as well as supply them with the updated state estimates of the MN so each node could search in the appropriate area for the next measurement angle.

For the proposed approach, the measurement noise covariance matrix, R_k, is a constant value, R_c, that was calculated in advance of the experiments by having the system try to scan the angles of the mobile node's position while the mobile node remained at a fixed location. The values of this matrix were found using 3 separate fixed positions, with each position selected to ensure that each base node pair equally contributed to the matrix, and with 50 measurements for each location so to best characterize the error of this 3 base node approach. The x and y errors generated from comparing the base node's measured position against these fixed positions were then fused together in the following formula to generate the matrix.

$$R_c = \begin{bmatrix} R_{x,x} & R_{x,y} \\ R_{y,x} & R_{y,y} \end{bmatrix} = \frac{1}{K}\begin{bmatrix} \sum_{k=1}^{K}(\tilde{x}_k - \mu_x)^2 & \sum_{k=1}^{K}(\tilde{x}_k - \mu_x)(\tilde{y}_k - \mu_y) \\ \sum_{k=1}^{K}(\tilde{y}_k - \mu_y)(\tilde{x}_k - \mu_x) & \sum_{k=1}^{K}(\tilde{y}_k - \mu_y)^2 \end{bmatrix} \quad (26)$$

where K is the total number of measurements the base nodes captured, $\tilde{x}$ and $\tilde{y}$ are the magnitudes of the errors for the x and y coordinates, respectively, and μ_x and μ_y are the average errors among all of the captured measurements for x and y, respectively.

Orientation data for the mobile node was captured by the NaturalPoint®'s OptiTrack motion tracking system. Strategically placed infrared cameras captured the location and orientation of the MN by cross referencing the positions of reflective markers attached to the MN as shown in Fig. 10. The MN would send and receive Universal Datagram Protocol (UDP) packets over Wi-Fi to get position and heading data from the PC running the motion tracking software. The position data received was used only as the ground truth position in post processing of the experiment's results.

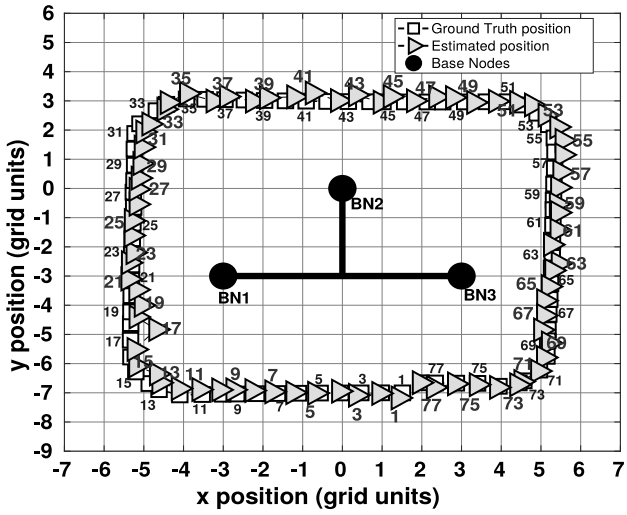

Fig. 12. Experimental results from one of the trials of the proposed minimal sensitivity with fixed-R approach. The plot shows the MN's estimated position plotted against the ground truth.

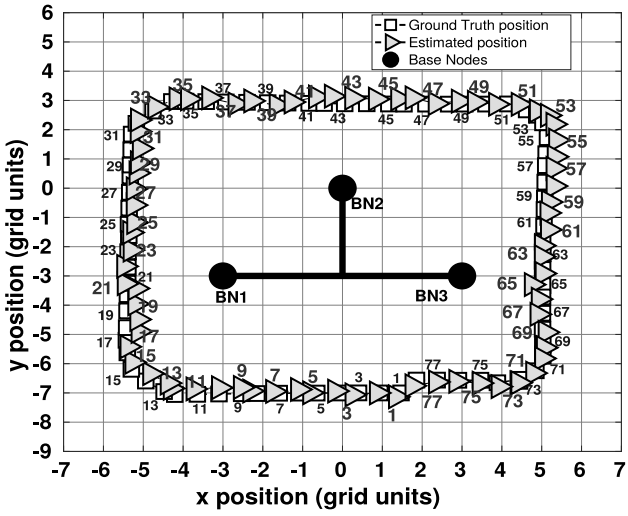

Fig. 13. Experimental results from one of the trials of the alternative minimal sensitivity with variable-R approach. The plot shows the MN's estimated position plotted against the ground truth.

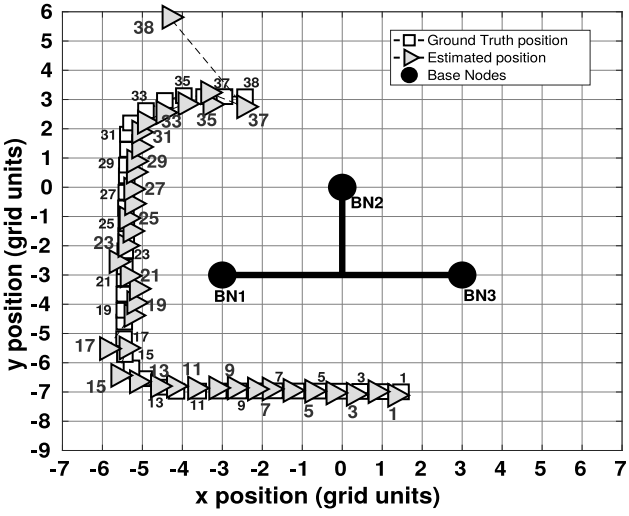

Fig. 14. Experimental results from one of the trials of the alternative averaging with fixed-R approach. The plot shows the MN's estimated position plotted against the ground truth.

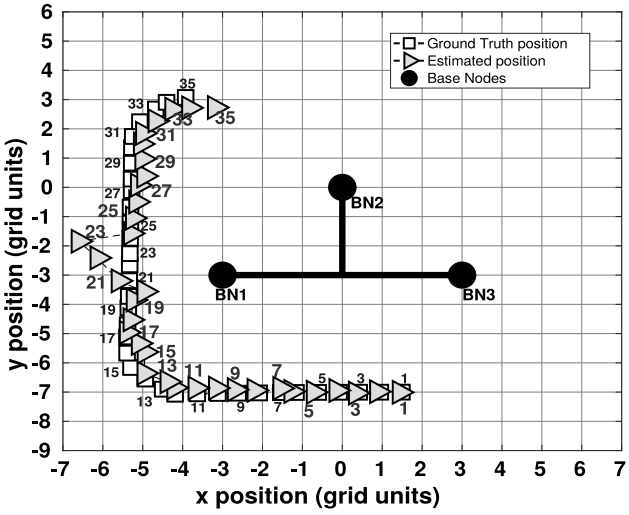

Fig. 15. Experimental results from one of the trials of the alternative averaging with variable-R approach. The plot shows the MN's estimated position plotted against the ground truth.

5.2. Results

Three experimental trials were conducted for each of the algorithm variations. Table 1 summarizes the performance for each algorithm variation across each of the three trials. In particular, it shows the mean and standard deviation of the estimated position error magnitude. Figs. 12, 13, 14, and 15 compare the estimated and ground truth positions of the mobile node along the x and y coordinates from one of the three trials for the minimal sensitivity with fixed-R, minimal sensitivity with variable-R, averaging with fixed-R, and averaging with variable-R approaches, respectively.

Collectively these results mirror the observations noticed in the simulation. In particular, both minimal sensitivity approaches have similar performance metrics, with the proposed fixed-R approach showing a slight advantage with a lower mean and standard deviation of its estimated position error. Both averaging based approaches significantly under-performed as both versions were unable to track the robot to the end of the trajectory. This is because the averaging approaches, unlike the minimal sensitivity approach, are unable to effectively mitigate the effect of large position measurement errors.

Table 1
Summarized experimental results from the three trials of each algorithm variation. The results include the mean and standard deviation of the estimated position error magnitude.

		Estimated position error	
		Mean	Standard deviation
Min. sensitivity	Fixed R	0.1813	0.0833
	Variable R	0.1998	0.1272
Averaged	Fixed R	0.2817	0.2245
	Variable R	0.2518	0.2738

6. Conclusion

This paper has presented the algorithm design and system implementation of a mobile robot LED-based optical localization system that uses a network of multiple beacon nodes to compute the coordinates of the robot. In particular, the proposed approach builds upon our previous two-beacon system which used the bearing angles needed to establish LOS communication between the beacons and the robot to compute the robot's measured position. To optimize data fusion from multiple beacons and improve the positioning process, a sensitivity metric has been proposed which characterizes the level of uncertainty in the computed position from the measured bearing angles of the beacons. The metric is used to select the optimal pair of beacons for the measured position. This approach overcomes the limitations of the two-base-node approach and enables a high level of localization accuracy. It is important to note that while our simulations and experiments are carried out with three base nodes, the proposed approach is easily extendable to work with groups containing more base nodes.

Simulated and experimental evaluations were conducted in a two-dimensional terrestrial setting, so to validate the proposed design without the numerous overhead concerns associated with three-dimensions (3D). For future work, we will expand this concept to the 3D setting and explore using more realistic dynamics of the mobile node (rigid-body dynamics instead of point mass dynamics) to enhance the system performance. Correspondingly, the system hardware will be improved and waterproofed for experimental evaluation in the underwater setting.

CRediT authorship contribution statement

Jason N. Greenberg: Conceptualization, Methodology, Software, Validation, Formal analysis, Investigation, Data curation, Writing - original draft, Writing - review & editing, Visualization. **Xiaobo Tan:** Conceptualization, Supervision, Project administration, Funding acquisition, Writing - review & editing, Resources.

Declaration of competing interest

The authors declare that they have no known competing financial interests or personal relationships that could have appeared to influence the work reported in this paper.

Acknowledgments

This work was supported by the National Science Foundation (ECCS 1446793, IIS 1734272). The first author would like to thank Dr. Dhrubajit Chowdhury for instrumental and inspiring discussions on this work.

References

[1] Kim M, Chong NY. RFID-based mobile robot guidance to a stationary target. Mechatronics 2007;17(4–5):217–29.

[2] Peula JM, Urdiales C, Sandoval F. Explicit coordinated localization using common visual objects. In: 2010 IEEE international conference on robotics and automation. 2010, p. 4889–94. http://dx.doi.org/10.1109/ROBOT.2010.5509398.

[3] Font-Llagunes JM, Batlle JA. Consistent triangulation for mobile robot localization using discontinuous angular measurements. Robot Auton Syst 2009;57(9):931–42.

[4] Pierlot V, Van Droogenbroeck M. A new three object triangulation algorithm for mobile robot positioning. IEEE Trans Robot 2014;30(3):566–77. http://dx.doi.org/10.1109/TRO.2013.2294061.

[5] Esteves JS, Carvalho A, Couto C. Generalized geometric triangulation algorithm for mobile robot absolute self-localization. In: 2003 IEEE international symposium on industrial electronics (Cat. No.03TH8692). 1, 2013, p. 346–51. http://dx.doi.org/10.1109/ISIE.2003.1267272.

[6] Sergiyenko O. Optoelectronic system for mobile robot navigation. Optoelectron Instrum Data Process 2010;46(5):414–28. http://dx.doi.org/10.3103/S8756699011050037.

[7] Rodríguez-Quiñonez JC, Sergiyenko O, Gonzalez-Navarro FF, Básaca-Preciado LC, Tyrsa V. Surface recognition improvement in 3D medical laser scanner using levenberg-marquardt method. Signal Process 2013;93(2):378–86. http://dx.doi.org/10.1016/j.sigpro.2012.07.001.

[8] Lindner L, Sergiyenko O, Rvias-López M, Hernández-Balbuena D, Flores-Fuentes W, Rodríguez-Quiñonez JC, et al. Exact laser beam positioning for measurement of vegetation vitality. Ind Robot 2017;44(4):532–41. http://dx.doi.org/10.1108/IR-11-2016-0297.

[9] Tekdas O, Isler V. Sensor placement for triangulation-based localization. IEEE Trans Autom Sci Eng 2010;7(3):681–5. http://dx.doi.org/10.1109/TASE.2009.2037135.

[10] Madsen CB, Andersen CS. Optimal landmark selection for triangulation of robot position. Robot Auton Syst 1998;23(4):277–92.

[11] Rui G, Chitre M. Cooperative multi-AUV localization using distributed extended information filter. In: 2016 IEEE/OES autonomous underwater vehicles (AUV). 2016, p. 206–12. http://dx.doi.org/10.1109/AUV.2016.7778673.

[12] Paull L, Seto M, Leonard JJ. Decentralized cooperative trajectory estimation for autonomous underwater vehicles. In: Intelligent robots and systems (IROS 2014), 2014 IEEE/RSJ international conference on. 2014, p. 184–91. http://dx.doi.org/10.1109/IROS.2014.6942559.

[13] Emokpae LE, DiBenedetto S, Potteiger B, Younis M. UREAL: Underwater reflection-enabled acoustic-based localization. IEEE Sens J 2014;14(11):3915–25.

[14] Gadre AS, Maczka DK, Spinello D, McCarter BR, Stilwell DJ, Neu W, et al. Cooperative localization of an acoustic source using towed hydrophone arrays. In: 2008 IEEE/OES autonomous underwater vehicles. 2008, p. 1–8. http://dx.doi.org/10.1109/AUV.2008.5290529.

[15] Anguita D, Brizzolara D, Parodi G. Building an underwater wireless sensor network based on optical: Communication: Research challenges and current results. In: 2009 third international conference on sensor technologies and applications. 2009, p. 476–9.

[16] Anguita D, Brizzolara D, Parodi G. Optical wireless communication for underwater wireless sensor networks: Hardware modules and circuits design and implementation. In: OCEANS 2010. 2010, p. 1–8. http://dx.doi.org/10.1109/OCEANS.2010.5664321.

[17] Rust IC, Asada HH. A dual-use visible light approach to integrated communication and localization of underwater robots with application to non-destructive nuclear reactor inspection. In: Robotics and automation (ICRA), 2012 IEEE international conference on. 2012, p. 2445–50. http://dx.doi.org/10.1109/ICRA.2012.6224718.

[18] Simpson JA, Hughes BL, Muth JF. Smart transmitters and receivers for underwater free-space optical communication. IEEE J Sel Areas Commun 2012;30(5):964–74. http://dx.doi.org/10.1109/JSAC.2012.120611.

[19] Solanki PB, Al-Rubaiai M, Tan X. Extended Kalman filter-aided alignment control for maintaining line of sight in optical communication. In: 2016 American control conference. 2016, p. 4520–5. http://dx.doi.org/10.1109/ACC.2016.7526064.

[20] Al-Rubaiai M. Design and development of an LED-based optical communication system (Master's thesis), Michigan State University; 2015.

[21] Solanki PB, Al-Rubaiai M, Tan X. Extended Kalman filter-based active alignment control for LED optical communication. IEEE/ASME Trans Mechatronics 2018;23(4):1501–11.

[22] Greenberg JN, Tan X. Efficient optical localization for mobile robots via Kalman filtering-based location prediction. In: Proceedings of the ASME 2016 dynamic systems and control conference. 2016; Minneapolis, MN, DSCC2016-9917.

[23] Greenberg JN, Tan X. Kalman filtering-aided optical localization of mobile robots: System design and experimental validation. In: Proceedings of the ASME 2017 dynamic systems and control conference. 2017; Tysons, VA, DSCC2017-5368.

[24] Greenberg JN, Tan X. Dynamic optical localization of a mobile robot using Kalman filtering-based position prediction. IEEE/ASME Trans Mechatronics 2020;25(5):2483–92. http://dx.doi.org/10.1109/TMECH.2020.2980434.

[25] Greenberg JN, Tan X. Optical localization of a mobile robot using sensitivity-based data fusion. In: 2019 IEEE/ASME International Conference on Advanced Intelligent Mechatronics (AIM). 2019; Hong Kong, China, 778–783.

[26] Reif K, Gunther S, Yaz E, Unbehauen R. Stochastic stability of the discrete-time extended Kalman filter. IEEE Trans Automat Control 1999;44(4):714–28. http://dx.doi.org/10.1109/9.754809.

[27] Rodríguez-Quiñonez JC, Sergiyenko O, Hernández-Balbuena D, Rivas-López M, Flores-Fuentes W, Básaca-Preciado LC. Improve 3D laser scanner measurements accuracy using a FFBP neural network with widrow-hoff weight/bias learning function. Opto-Electron Rev 2014;22(4):224–35. http://dx.doi.org/10.2478/s11772-014-0203-1.

Jason Greenberg received the B.S. degree in computer engineering from the State University of New York (SUNY) at New Paltz in 2012. He is currently working toward the Ph.D. degree in electrical and computer engineering at Michigan State University, East Lansing, MI, USA. His research focuses on localization of a mobile robot using the bearing angle from an LED-based optical communication system for underwater applications.

Xiaobo Tan received the B.Eng. and M.Eng. degrees in automatic control from Tsinghua University, Beijing, China, in 1995 and 1998, respectively, and the Ph.D. degree in electrical and computer engineering from the University of Maryland, College Park, in 2002. From September 2002 to July 2004, he was a Research Associate with the Institute for Systems Research at the University of Maryland. He joined the faculty of the Department of Electrical and Computer Engineering at Michigan State University (MSU) in 2004, where he is currently an MSU Foundation Professor. His research interests include modeling and control of systems with hysteresis, electroactive polymer sensors and actuators, soft robotics, and bio-inspired underwater robots and their application to environmental sensing. Dr. Tan has served as an Associate Editor/Technical Editor for Automatica, IEEE/ASME Transactions on Mechatronics, and International Journal of Advanced Robotic Systems. He has served as the Program Chair of the 2011 International Conference on Advanced Robotics and the General Chair of the 2018 ASME Dynamic Systems and Control Conference. He has coauthored one book (Biomimetic Robotic Artificial Muscles) and over 200 peer-reviewed journal and conference papers, and holds three US patents. He is a Fellow of IEEE, and a recipient of NSF CAREER Award (2006), MSU Teacher-Scholar Award (2010), MSU College of Engineering Withrow Distinguished Scholar Award (2018), Distinguished Alumni Award from the Department of Electrical and Computer Engineering at University of Maryland (2018), and several best paper awards.